JOURNAL OF MATERIALS SCIENCE 24 (1989) 1133–1139

Characterization of industrial materials by small angle X-ray scattering

YUJI SASANUMA, YUKISHIGE KITANO, AKIRA ISHITANI
Toray Research Center, Inc., 1-1, Sonoyama 1-Chome, Otsu, Shiga 520, Japan

Small angle X-ray scattering (SAXS) techniques have enabled remarkable progress to be made in both the experimental devices and algorithms of data processing. We have applied SAXS to the characterization of common industrial materials such as carbon fibres, γ-alumina, and polypropylene films. For carbon fibres, the microporosity has been investigated by estimating the cross-sectional dimensions of the microvoids in the powdered specimens as well as in the aligned fibre bundles. The average particle size of γ-alumina has been evaluated, and related to the heat-treatment conditions. Correlation-function analysis has revealed the changes in lamellar structure of polypropylene films induced by annealing. SAXS is shown to have the potential to be widely used as a practical method for characterizing materials of industrial importance.

1. Introduction

Fundamental theories of small angle X-ray scattering (SAXS) have been developed since the late 1930's. The early theoretical studies were published in the 1950's and 1960's [1–3]. In spite of this early establishment of the theoretical basis SAXS techniques have not been extensively used for characterization of industrial materials because of technical difficulties. The X-ray generators were not powerful enough to give easily counted scattered X-rays. Complicated numerical calculations have to be made in the processing of the measured intensity, for example collimation corrections and Fourier transformations. Thus, SAXS was considered time-consuming and impractical for daily use.

There is an area where SAXS has been extensively used, notwithstanding the difficulties [4–6]. Semicrystalline polymers such as polyolefines, polyamides, and polyesters have been well studied by the two-dimensional SAXS pattern recorded on photographic films. In this particular case, the scattering intensity is so strong that the experiment can be performed with a pinhole-collimation geometry. Since the scattering observed from the polymers can be considered similar to diffraction, the long periods of the lamellar structure can easily be calculated using Bragg's equation. Therefore, powerful X-ray sources and elaborate data processing have not been necessary in such studies.

Recently, a high-power X-ray generator with a rotating anode and a high-speed digital computer has become commercially available. In addition, position-sensitive detectors (PDSs) provide data with considerably improved signal-to-noise ratio, because a PSD can simultaneously accumulate intensities within the whole scattering range. Thus, SAXS has acquired the potential to be used for the characterization of industrial materials, as well as for academic research.

In the present paper, materials of industrial importance have been characterized to demonstrate the potential of SAXS in the present state-of-the-art [7]. The samples used in this study are carbon fibres, γ-alumina powders, and polypropylene films.

Since carbon fibres became commercially available, SAXS has been extensively used to study the structure of microvoids and microfibrils [8-13]. The SAXS studies on carbon fibres have attracted more attention recently, with an increase in their demand as a promising new material [14, 15]. We have investigated by SAXS the microporosity of carbon fibres produced from polyacrylonitrile fibres.

γ-alumina has been widely used as a dehydrating catalyst or a catalyst support. It is well known that particle size is important for catalytic activity. In previous work, the particle-size distribution of γ-alumina was estimated by a graphical analysis of a Guinier plot [16, 17]. Thereafter, methods to determine the particle-size distribution were developed [18–23]. In the present study, the structural parameters evaluated for γ-alumina will be discussed in relation to the conditions of sample preparation.

The morphological study of semicrystalline polymers is one of the major areas where SAXS has been advantageously applied. Methods for the analysis can be classified mainly into three types: simple calculations of the long periods by Bragg's equation, interpretations based on model calculations [24–27], and the evaluation of structural parameters from the correlation function [28, 29]. We have employed correlation-function analysis to study the change of the lamellar structure of a polypropylene film by annealing.

2. Theory

Small angle X-ray scattering is divided into continuous and discontinuous, i.e. single-particle and interference scattering. If the particles are widely

0022–2461/89 $03.00 + .12

separated from each other, they can be assumed to contribute independently to the scattering intensity. For example, particles dispersed in a dilute solution give rise to continuous scattering. According to the Babient theorem of reciprocity, complementary objects like vacant cavities produce the same effect. The continuous-scattering intensity decreases monotonously with increasing scattering angle.

On the other hand, discontinuous scattering results from the interference effect by dense packing and long-range order. There a scattering curve shows the first-order and occasionally the higher-order maxima, which can be looked upon as the diffraction peaks.

2.1. Distance distribution function

If the distribution of particles is statistically isotropic, and they have no long-range order, the scattering intensity is given as [30]

$$I(h) = 4\pi \int_0^\infty p(r) \frac{\sin(hr)}{hr} \, dr \quad (1)$$

In Equation 1, r denotes the distance in real space, and h is the magnitude of the reciprocal-space vector, $(4\pi/\lambda) \sin\theta$, where θ is a half of the scattering angle, and λ is the X-ray wavelength. If $I(h)$ is measured, the distance distribution function $p(r)$ is obtained by the Fourier transform

$$p(r) = \frac{1}{2\pi^2} \int_0^\infty I(h)(hr) \sin(hr) \, dh \quad (2)$$

The distance distribution function has the physical meaning of the autocorrelation of the electron density. Therefore, it can also be evaluated theoretically, by assuming the shape, dimension, and electron-density distribution of a particle. For example, the distance distribution function for a hard sphere having a homogeneous electron density is

$$p(r) = 12x^2(2 - 3x + x^3); \quad x = \frac{r}{D} \quad (3)$$

where D is the diameter of the sphere [31]. This function has its maximum at

$$x_{max} = r_{max}/D = 0.525 \quad (4)$$

The value of r_{max} is estimated from the $p(r)$ function obtained by the numerical calculation of Equation 2. Substitution of the value r_{max} in Equation 4 yields the diameter of the spherical particle. In a high concentration of particles, the interparticle–interference effect is not negligible. Consequently, the $p(r)$ function is somewhat distorted. Nevertheless, model calculations have shown that Equation 4 holds approximately even in such dense systems [32].

2.2. Radius of gyration

At small angles, the scattering curve can be adequately approximated by a Gaussian function of h. This is well known as Guinier's law which is expressed by

$$I(h) = I(0) \exp\left(-\frac{R^2h^2}{3}\right) \quad (5)$$

where $I(0)$ is the scattering intensity at $h = 0$, and R the so-called radius of gyration [1, 33]. When $\ln I(h)$ is plotted against h^2, R can be determined from its slope. The radius of gyration of the particle is considered as the mean square distance from the electronic centre of gravity. Therefore, R can be determined for homogeneous particles. For example, R of a spherical particle is a function of the diameter D

$$R^2 = \frac{3}{20} D^2 \quad (6)$$

In addition, the radius of gyration can be obtained from the $p(r)$ function [1]

$$R^2 = \frac{\int_0^\infty p(r) r^2 \, dr}{2\int_0^\infty p(r) \, dr} \quad (7)$$

2.3. Correlation length

If a straight line is drawn through a particle, a segment of the line is cut by the contours of the particle. The correlation length l_c is the average length of all segments of lines drawn through all points of the particle in all directions. The correlation length is obtainable from the scattering intensity as in Equation 8 [34, 35].

$$l_c = \frac{\pi \int_0^\infty I(h)h \, dh}{\int_0^\infty I(h)h^2 \, dh} \quad (8)$$

2.4. Distance distribution function of the cross section

The distance distribution function of the cross section of a rod-like particle $p_c(r)$ is given by

$$p_c(r) = \frac{1}{2\pi} \int_0^\infty I_c(h)(hr)J_0(hr) \, dh \quad (9)$$

where $J_0(hr)$ is the zero-order Bessel function [36]. The scattering intensity of the cross section $I_c(h)$ can be related to the scattering intensity for particles having an isotropic orientation $I(h)$ [31]

$$I_c(h) \propto I(h)h \quad (10)$$

The analytical expression of the $p_c(r)$ function for a homogeneous circular cylinder is given by

$$p_c(r) = \text{constant } x(\arccos(x) - x\sqrt{1 - x^2})$$
$$x = \frac{r}{D_c} \quad (11)$$

where D_c is the diameter of the cross-section [31]. The maximum of this function is found at

$$x_{max} = r_{max}/D_c = 0.418 \quad (12)$$

Therefore, the cross-sectional diameter of a circular cylinder can be estimated by the maximum position of the $p_c(r)$ function, using Equation 12.

2.5. Correlation function for lamellar structure

The periodic lamellar structure of alternating crystalline and amorphous regions in semicrystalline polymers gives rise to discontinuous scattering. The lamellar structure has often been studied with the aid of the autoconvolution of the electron density. The autoconvolution is called the correlation function. The correlation function $\gamma(r)$ for the lamellar structure

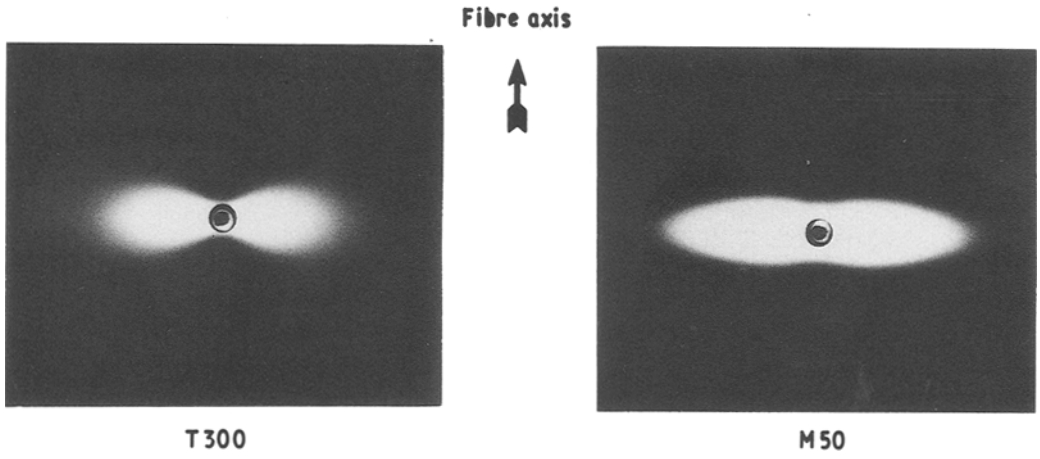

Figure 1 Small angle X-ray scattering patterns of commercial carbon fibres.

is usually scaled by setting its value as unity at $r = 0$. The $\gamma(r)$ function is obtained directly from the Fourier transform of the scattering intensity [28]

$$\gamma(r) = \frac{\int_0^\infty I_t(h) \cos(hr)\, dh}{\int_0^\infty I_t(h)\, dh} \quad (13)$$

where $I_t(h)$ is the scattering intensity parallel to the stacking direction of the lamellae, and is given by the isotropic three-dimensional intensity $I(h)$ [31]

$$I_t(h) \propto I(h)h^2 \quad (14)$$

2.6. Desmearing

Small angle X-ray scattering experiments are usually performed with slit collimation to increase the scattered intensity, instead of with the pinhole collimation. However, the scattering intensity thus obtained is very different from that with pinhole collimation. Before the transformations described above are applied, the measured intensity must be converted into the pinhole-like intensity. The procedure is called desmearing which mainly comprises slit-length, slit-width, and non-monochromaticity corrections. When collimation systems with narrow slit-width as in a Kratky camera, and well-monochromatized incident beams are used, only the effect of the slit-length is necessary to be considered. In the past few decades, many reports describing desmearing procedures have been published. Recently, the exact solution of the slit-length effect has been successfully obtained by Deutsch and Luban [37–39]. We have employed it for the slit-length correction, using the rectangular slit function.

3. Experimental procedure

3.1. Materials

Carbon fibres and graphite fibres commercially available from Toray Industries, Inc., Torayca, were used in the present study. The filaments aligned parallel to one another were formed into a bundle of rectangular cross section by using a small amount of adhesive.

The raw material of aluminium oxide was prepared by mixing aluminium hydroxide with a small amount of silica. Two series of heat treatments were adopted. In the first series, aluminium hydroxide was heated up to temperatures of 1000, 1150, 1200 and 1230° C with the same heating rate of 400° C h^{-1}; in the second series, up to 1150° C with different rates of 400, 800, and 1200° C h^{-1}. After heating, all samples were identified as γ-alumina by the X-ray powder diffraction.

Samples of polypropylene films were prepared as follows. Melt-extruded polypropylene was elongated approximately 35 times, and immersed into a water bath at 70° C (as extruded sample). In addition, an extruded film was annealed at 140° C for one minute (annealed sample). Strips of the films were stacked about 1 mm thick for measurements.

3.2. Apparatus and measurement

Small angle X-ray scattering measurements were carried out with a Kratky camera. The width of the entrance slit was 70 μm. The incident X-ray beam was produced by a rotating-anode generator operated at 40 kV and 200 mA, and then monochromatized by a graphite crystal. The scattered X-rays were detected by a position-sensitive proportional counter (PSPC) with a pulse-height discriminator. The resolution of the PSPC was 0.022° per unit channel.

Also, small angle X-ray scattering photographs were taken with a Kiessig camera. Nickel-filtered Cu K_α radiation generated by a rotating anode at 50 kV and 150 mA was used. The distance between the sample and photographic film was 400 mm.

The observed scattering intensity was smoothed by the Savitzky–Golay method [40, 41]. Scattering data within a small angular range were evaluated by extrapolation, using polynomials determined by a least-squares fitting. Background scattering was estimated from the slope of the Ih^3 against h^3 plot [34, 42]. Background scattering was subtracted for the observed data using a LSI-11/23 computer.

4. Results and discussion

4.1. Carbon fibres

The small angle X-ray scattering photograph of

TABLE I Dimensions of cross-sections of microvoids for commercial carbon fibres

Sample	Fibre specimen		Powdered specimen
	l_c(nm)	D_c(nm)	D_c(nm)
T300	1.67	2.38	2.11
T400	1.77	2.48	2.18
T700	1.78	2.47	2.21
M40	2.61	3.16	2.81
M50	3.17	4.11	3.12

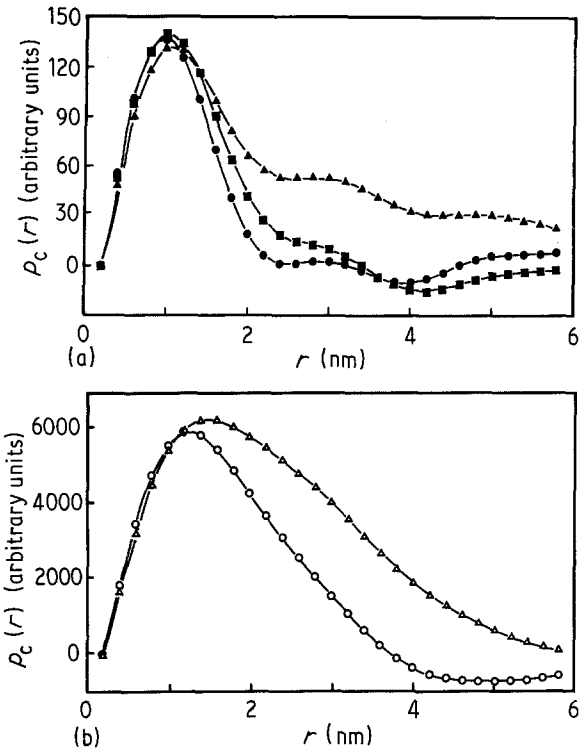

Figure 2 Distance distribution functions of the cross-section for commercial (a) carbon fibres and (b) graphite fibres: ● T300; ▲ T400; ■ T700; ○ M40; △ M50.

uniaxially oriented carbon fibres shows a strong butterfly-like streak as indicated in Fig. 1. According to the Babinet principle of reciprocity, cavities in a dense matrix produce the same effects as particles dispersed in a light-density medium. The SAXS of carbon fibres is known to arise from the microvoids among the graphitized micro-fibrils [43, 44]. The microvoids have a needle-like shape or a slender cylinder elongated along the fibre axis. The equatorial SAXS

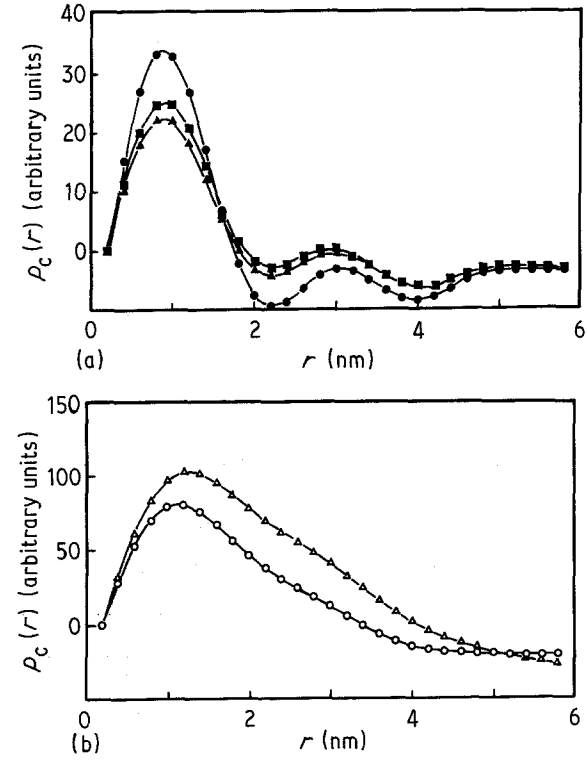

Figure 3 Distance distribution functions of the cross-section for powdered specimens of commercial (a) carbon fibres and (b) graphite fibres: ● T300;▲ T400; ■ T700; ○ M40; △ M50.

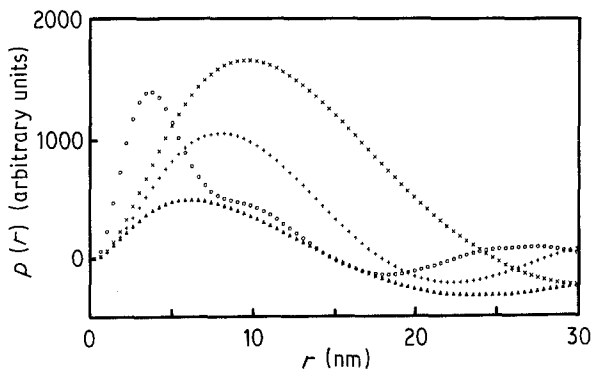

Figure 4 Distance distribution functions for γ-alumina containing 5 wt % of silica. The annealing temperatures are; ○ 1000° C; △ 1150° C; + 1200° C; x 1230° C. The temperature was raised with 400° C h^{-1}.

profile contains information on the shape and size of the cross-sections of the microvoids. The correlation length of the cross-sections can be estimated from the desmeared equatorial intensity by using Equation 8. If the cross-sections can be assumed to be circular, then the average diameter can be evaluated from the maximum of $p_c(r)$ of Equation 9. The $p_c(r)$ functions are shown in Fig. 2. The structural parameters obtained from these measurements are summarized in Table I.

The average diameters of the cross-sections of the voids were also estimated for isotropic powder specimens prepared by grinding carbon fibres. An accurate evaluation for the isotropic specimens is important for the application of SAXS techniques to carbon fibre composites from which it is difficult to extract filaments. A powdered specimen can easily be prepared even from such carbon fibre composites. By assuming that the voids are cylindrical, the average diameters of the voids were also estimated from the maxima of $p_c(r)$ calculated using Equations 9 and 10. The results are given in Table I.

From early studies, the correlation length evaluated by Debye's method [30, 45] or the numerical calculation of Equation 8 has often been used as a convenient measure of the cross-sectional dimensions of the microvoids [8–10]. The values obtained, ranging from 1 to 4 nm, are in good agreement with those in this study. In both fibre and powdered specimens, the dimensions are found to increase, as the baking temperature increases. On the whole, however, values of

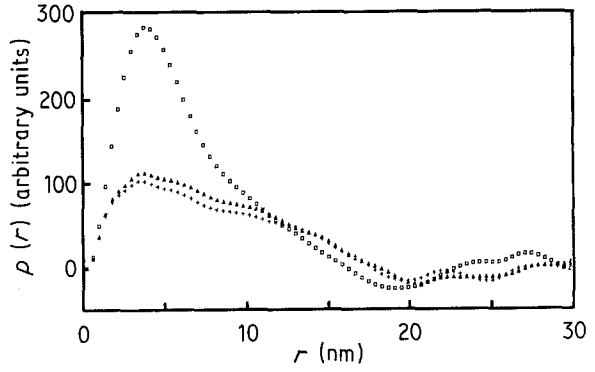

Figure 5 Distance distribution functions for γ-alumina containing 10 wt % of silica. The samples were heated up to 1150° C. The rates of elevation of the temperature are: □ 400° C h^{-1}; △ 800° C h^{-1}; + 1200° C h^{-1}.

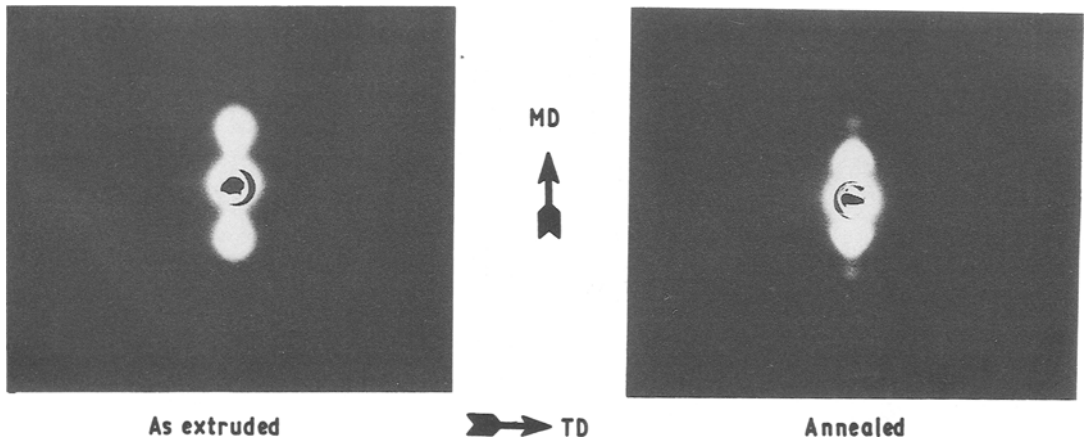

Figure 6 The small angle X-ray scattering patterns of the polypropylene films. (MD) machine direction; (TD) transverse direction.

the average diameters obtained from powdered specimens are smaller than those from fibre bundles, although they agree well for most of the samples. The difference between the diameters for both samples is significant, particularly in the graphite fibre, M50, which was treated at the highest temperature. The graphitization of the crystalline region and also the growth of the microvoids is expected to proceed with increasing baking temperatures. The extended microvoids may be broken in M50 by grinding. Perret and Ruland also suggested that the microstructure of brittle carbon fibres may be changed by grinding [12]. However, we have indicated in this study that the grinding method can be applied at least to carbon fibres treated at relatively low temperatures.

4.2. γ-alumina

Fig. 4 shows the distance distribution functions of the first series of γ-alumina samples which contain 5 wt % of silica. Annealing temperatures range from 1000 to 1230° C. The $p(r)$ function for 1000° C has a distinct peak at 3.6 nm and also a discernible shoulder at about 10 nm. This means that the sample comprises two groups of particle sizes. By assuming spherical particles, the average diameters for the two groups are determined from Equation 4 to be 6.8 and 19 nm respectively. The radius of gyration calculation gives an overall average diameter of 11.2 nm, which is intermediate between those obtained from the $p(r)$ function.

On the other hand, such a shoulder disappears in $p(r)$ of samples treated at temperatures higher than 1150° C. As the temperatures rises, the peak of $p(r)$ shifts to a larger distance, and becomes more symmetrical. Such changes in $p(r)$ imply the growth of particles into a single dispersed system by temperature elevation. The average diameters estimated from radii of gyration and $p(r)$ are summarized in Table II.

TABLE II Dimensions of γ-alumina particles evaluated from small angle X-ray scattering

Annealing temperature (° C)	R (nm)	Average diameter of particles (nm)	
		From $p(r)$	From R
1000	4.37	6.8, 19.0	11.2
1150	5.93	11.7	15.3
1200	6.44	15.4	16.6
1230	8.45	18.4	21.8

The second series of γ-alumina samples contained 10 wt % of silica. The temperatures of the samples were raised with different rates of 400, 800, and 1200° C h^{-1}. The final temperature is 1150° C, common to the three samples. The $p(r)$ functions of the samples are shown in Fig. 5. The curve for the rate of 400° C h^{-1} has a sharp peak at 4 nm, implying that the particle-size distribution is narrow. The $p(r)$ function changes into a broader and more complicated curve, as the rate increases. This behaviour can be considered to come from overlapping of the various distance-distribution functions corresponding to different-size particles. The change in $p(r)$ indicates that the particle sizes become more irregular with increasing heating rate. The particle-size and its uniformity may be related to the various properties of γ-alumina in practical use, for example mechanical strength, specific surface area, and catalytic activity.

4.3. Polypropylene films

In the two-dimensional SAXS patterns of polypropylene films, the interference scattering appears in the shape of "drops" or "globules" along the machine direction (MD), the direction of elongation. According to model calculations by Tsvankin and co-workers [26, 27], such shapes of the interference scattering arise from planar lamellar structure in which the lamellae are stacked along the MD. Therefore, the scattering intensity along the MD contains information about the way of lamellar stacking. As shown in Fig. 6, a second-order maximum is also observed in the SAXS pattern of the annealed film, while only the first-order

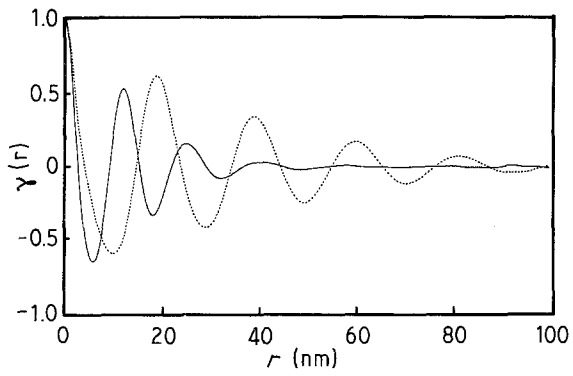

Figure 7 The one-dimensional correlation functions for the polypropylene films, derived from the scattering intensity along MD. —— as extruded; – – –annealed.

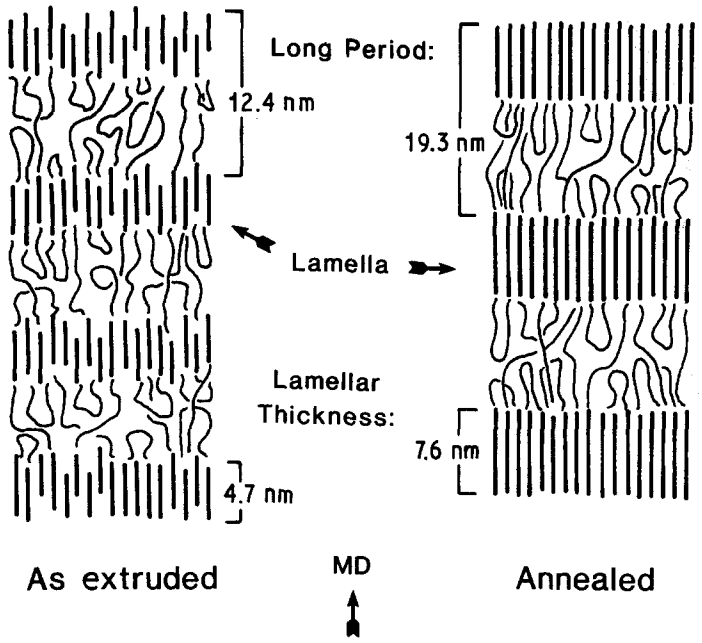

Figure 8 A schematic representation of the lamellar systems of the polypropylene films. The correlation-function analysis reveals increases of the long period and the lamellar thickness, and also increment of structural regularity by annealing.

maximum appears in the as-extruded film. This indicates that annealing increases the regularity in the lamellar stacking. The difference between the lamellar structures of the films becomes clearer by a correlation-function analysis.

Fig. 7 shows the one-dimensional correlation functions given by Equation 13. From a correlation function, one can estimate the parameters to characterize the lamellar structure. A regular sequence of maxima is observed. The first maximum reflects the correlation within a lamella (the self-correlation), the second corresponds to the nearest neighbours, and the third to the next-nearest neighbours, and so on. The position of the first peak corresponds to the average distance between the adjoining lamellae, i.e., the long period. If the ideal two-phase model [29] is assumed, one can obtain the average lamellar thickness. Since the peak height represents the correlation between the neighbouring lamellae, the rate of peak-height decay can be regarded as a measure of the regularity in the lamellar structure. As regularity of the lamellar stacking increases, the peak height decay decreases. Consequently, the regularity of lamellar structures of the films can be schematically represented in Fig. 8, together with values of the long period and lamellar thickness.

5. Acknowledgement

This study was performed through Special Coordination Funds of the Science and Technology Agency of the Japanese Goverment.

References

1. A. GUINIER and G. FOURNET, "Small-Angle Scattering of X-rays" (Wiley, New York, 1955).
2. O. KRATKY, in "Progress in Biophysics", Vol. 13 (Pergamon Press, New York, 1963) p. 105.
3. H. BRUMBERGER, "Small-Angle X-ray Scattering" (Gordon and Breach, New York, 1967).
4. K. HESS and H. KIESSIG, *Z. Phys. Chem.* **193** (1944) 196.
5. O. KRATKY, *J. Polym. Sci.* **3** (1948) 195.
6. D. HEIKENS, P. H. HERMANS and A. WEIDINGER, *Nature* **170** (1952) 369.
7. O. GLATTER and O. KRATKY, "Small Angle X-ray Scattering" (Academic Press, London, 1982).
8. D. J. JOHNSON and C. N. TYSON, *J. Phys. D* **2** (1969) 787.
9. *Idem., J. Phys. D* **3** (1970) 526.
10. R. PERRET and W. RULAND, *J. Appl. Crystallogr.* **1** (1968) 308.
11. W. RULAND, *J. Polym. Sci. C* **28** (1969) 143.
12. R. PERRET and W. RULAND, *J. Appl. Crystallogr.* **2** (1969) 209.
13. Idem., ibid. 3 (1970) 525.
14. M. SHIOYA and A. TAKAKU, *J. Appl. Phys.* **58** (1985) 4074.
15. MING-YA TANG, G. G. RICE, J. F. FELLERS and J. S. LIN, *ibid.* **60** (1986) 803.
16. M. H. JELLINEK and I. FANKUCHEN, *Ind. Eng. Chem.* **37** (1945) 158.
17. M. H. JELLINEK, E. SOLOMON and I. FANKUCHEN, *ibid.* **38** (1946) 172.
18. C. G. SHULL and L. C. ROESS, *J. Appl. Phys.* **18** (1947) 295.
19. L. C. ROESS and C. G. SHULL, *ibid.* **18** (1947) 308.
20. G. F. NEILSON, *J. Appl. Crystallogr.* **6** (1973) 386.
21. C. G. VONK, *ibid.* **9** (1976) 433.
22. I. S. FEDOROVA and P. W. SCHMIDT, *ibid.* **11** (1978) 405.
23. O. GLATTER, *ibid.* **13** (1980) 7.
24. R. HOSEMANN and S. N. BAGCHI, "Direct Analysis of Diffraction by Matter" (North-Holland, Amsterdam, 1962).
25. R. HOSEMANN, *J. Appl. Phys.* **34** (1963) 25.
26. V. I. GERASIMOV and D. YA. TSVANKIN, *Vysokomol. Soed.* **A11** (1969) 2652.
27. V. I. GERASIMOV, YA. V. GENIN and D. YA. TSVANKIN, *J. Polym. Sci., Polym. Phys. Edn* **12** (1974) 2035.
28. C. G. VONK and G. KORTLEVE, *Kolloid Z. Z. Polym.* **220** (1967) 19.
29. G. R. STROBL and M. SCHNEIDER, *J. Polym. Sci., Polym. Phys. Edn.* **18** (1980) 1343.
30. P. DEBYE and A. M. BUECHE, *J. Appl. Phys.* **20** (1949) 518.
31. G. POROD, *Acta Phys. Austriaca* **2** (1948) 255.
32. O. GLATTER, *J. Appl. Cryst.* **12** (1977) 166.
33. A. GUINIER, *Ann. Phys.* **12** (1939) 161.
34. G. POROD, *Kolloid Z.* **124** (1951) 83.
35. *Idem., ibid.* **125** (1952) 51.
36. B. A. FEDOROV and V. G. ALESHIN, *Vysokomol. Soed.* **8** (1966) 1506.
37. M. DEUTSCH and M. LUBAN, *J. Appl. Crystallogr.* **11** (1978) 87.

38. *Idem., ibid.* **11** (1978) 98.
39. M. LUBAN and M. DEUTSCH, *ibid.* **13** (1980) 233.
40. A. SAVITZKY and M. J. E. GOLAY, *Anal. Chem.* **36** (1964) 1627.
41. J. STEINIER, Y. TERMONIA and J. DELTOUR, *ibid.* **44** (1972) 1906.
42. V. LUZZATI, *Acta Crystallogr.* **13** (1960) 939.
43. R. E. FRANKLIN, *ibid.* **3** (1950) 107.
44. R. E. FRANKLIN, *Proc. R. Soc. A* **209** (1951) 196.
45. P. DEBYE, H. R. ANDERSON and H. BRUMBERGER, *J. Appl. Phys.* **28** (1957) 679.

Received 18 February
and accepted 14 June 1988